Bayesian optimization approach to model-based description of α decay

Zisheng Jin,[1,*] Mingshuai Yan,[1,*] Hao Zhou,[1] An Cheng,[2] Zhongzhou Ren,[3] and Jian Liu ⬤[1,4,5,†]

[1]*College of Science, China University of Petroleum (East China), Qingdao 266580, China*
[2]*Department of Physics, Nanjing University, Nanjing 210093, China*
[3]*School of Physics Science and Engineering, Tongji University, Shanghai 200092, China*
[4]*The Key Laboratory of High Precision Nuclear Spectroscopy, Insititute of Modern Physics,*
Chinese Academy of Sciences, Lanzhou 730000, China
[5]*Guangxi Key Laboratory of Nuclear Physics and Nuclear Technology, Guangxi Normal University, Guilin 541004, China*

α decay serves as an important probe for the studies of unstable nuclei. This paper proposes an approach combining the sophisticated α-decay model and Bayesian neural network (BNN) to improve the prediction accuracy of α-decay half-lives. The global and extrapolated analyses show that the BNN method can improve the description of model-based predictions of α decay. In our calculation, the experimental decay energies Q_α are used to obtain the accurate α-decay penetration probability, which indicates that the improvements come from the corrections of α-cluster preformation factors. Further analyzing α-decay half-lives of nuclide chains shows that the shell structure effect can be well introduced into estimations of α-cluster preformation factors by utilizing the BNN. The studies of this paper provide an effective way to predict the α-decay half-lives of unknown nuclei.

I. INTRODUCTION

α decay has been one of the most important modes of nuclear decay for more than a century. As a time-dependent quantum many-body problem, α decay is critical to improve the contemporary nuclear models and study the structure of exotic nuclei [1,2]. Meanwhile, it plays a vital role in identifying newly synthesized superheavy elements or new isotopes [3,4]. In astrophysics, the α decay of ^{146}Sm has been used as a clock to measure the formation of the solar system [5]. As the significant decay mode, one can extract rich structural information from α decay about the nuclear deformation [6,7], effective nuclear interaction [8,9], shell effects [10,11], α clustering [12–14], etc.

The α-decay process can be described as a tunneling effect of an α particle through the barrier formed by both the attractive nuclear potential and the repulsive Coulomb potential [15,16]. Based on this simplification, the investigations of α decay are divided into two main elements: the calculations of the α-decay penetration probability and the estimations of α-cluster preformation factor P_α. Various theoretical models have been proposed to determine the α-decay penetration probability, such as the two-potential approach [17,18], the deformed tunneling model [19,20], and the multichannel cluster model [21]. Compared with the penetration probability, the treatment of α-cluster formation in the parent nucleus is more complicated, which is at least a quantum five-body problem as one needs to handle not only the internal motion for the four

nucleons in the cluster but also the relative motion between the cluster and the core [22–25]. Despite many efforts [26–33], the α-cluster formation problem in α-decay theory has not been completely understood.

The α-cluster preformation factor P_α is usually considered as a constant empirically for a certain type of parent nuclei. This simplistic treatment is because the P_α varies smoothly throughout the open shell region [8], but such an assumption is possibly insufficient to accurately reproduce the half-lives close to the shell closure. There are significant changes on the P_α across the closed shells, such as the proton $Z = 82$ and the neutron $N = 126$ [34,35]. In previous researches, a limited number of semiempirical formulations were proposed including the impacts of nucleon configuration and shell structure [36,37], such as the number of valence nucleons and quartets above the closest doubly magic nuclei [38], the fragmentation potential [22], and the daughter mass number [39]. Based on the difference in binding energy between parent and neighboring nuclei, the cluster-formation model (CFM) has also been proposed to extract the P_α through a systematics of separation energy [40,41].

At the microscopic level, α preformation factors can be calculated by overlapping between the α-decay wave function and the primal wave function. For light nuclei, there have been a lot of successful studies in the α-like correlations employing microscopic methods, such as the fermionic molecular dynamics (FMD) model and quantum Monte Carlo (QMC) method [42–46]. However, complete microscopic computations are difficult and time-consuming for heavy nuclei. The present microscopic studies have presented the P_α for few benchmark nuclei like ^{104}Te and ^{212}Po by using the quartetting wave-function approach [24,47]. This work aims to employ

the machine learning approach to provide the value of the P_α for wide region of α emitters.

As a statistical model, the machine learning provides a new extended approach to process nuclear systems and to complement the quantum theory-based models [48]. The study of nuclear structure and reaction has benefited greatly in recent years by the participation of numerous machine learning techniques, like the Gaussian process (GP) [49,50], the naive Bayes classifier (NBP) [51,52], the deep learning (DL) [53,54], the restricted Boltzmann machines (RBMs) [55,56], and the Bayesian neural networks (BNN) [57,58]. It is favored by physics researchers due to its ability to extract key information about the underlying scientific laws and physical processes based on massive datasets. The BNN has excellent advantages, including the estimation of errors, automatic complexity control, as well as avoiding overfitting [59,60], which has been used effectively in nuclear physics to predict nuclear radii [61,62], nuclear masses [63,64], and β-decay half-lives [65,66]. Note that the BNN is also utilized to refine the theoretical Q_α from the mass models [67,68].

In this paper, by employing the Bayesian neural network, we systematically investigate the estimations of α-decay width and demonstrate that the BNN method can refine the α-cluster preformation factor P_α. Note that analyzing the α emitters of isotopic and isotonic chains, the influences of shell structure effect on P_α are further explored to show the ability of the BNN method in refining α-decay width. There are two integrants in this work. Primarily, four inputs, namely the proton number Z, the α-decay energy Q_α, the asymmetric coefficient S, and the change in angular momentum l, are selected to refine the α-decay half-lives. Secondly, the experimental Q_α is used instead of the theoretical values from the nuclear mass models to calculate raw α-decay half-lives. Experimental Q_α guarantees the accurate calculations of α-decay penetration probability, thus the improvements are mainly from the P_α corrections using BNN. In order to illustrate the generality of the BNN method, we choose three α-decay models including the spherical tunneling model [69], the deformed tunneling model [19], and a semiempirical formula [70] to calculate the raw α-decay half-lives. In total, there are 420 experimental α emitters with well-defined branching ratios in the Nudat3.0 [71]. Based on this database, the data set contains 479 data. It includes all the 420 α-decay transition data from the ground state to the ground state. For the 59 parent nuclei whose ground states have different J^π from those of the daughter nuclei, the decay channels with largest branching ratios are also contained in the data set.

It should be pointed out that the previous theoretical α-decay models mainly focus on the research of favored α transitions and have achieved good agreement with the experimental data. However, for some odd-A nuclei and odd-odd nuclei, the transitions from ground state to ground state are unfavored α transitions, and studies on these transitions are sparse. If the previous theoretical models are directly generalized to the unfavored α transition, it is expected that the bias will be large. Therefore, we apply a machine learning method to favored and unfavored transitions to extend the studies on α decay. Numerous and precise experimental data of favored transitions are helpful in substantially improving the accuracy

of BNN predictions. By introducing changes in angular momentum as input variables, BNN is able to analyze and reveal the underlying nuclear structure correlations associated with unfavored transitions.

This paper is organized in the following way. In Sec. II, the framework of α-decay models and BNN method are presented. The results and corresponding discussions are provided in Sec. III. Finally, a summary is given in Sec. IV.

II. THEORETICAL FRAMEWORK

In this section, we introduce two tunneling models including the spherical tunneling model and the deformed tunneling model for calculating the $T_{1/2}$. Then, we further present the framework of the BNN method, which shows the construction of the network.

A. α-decay models

In the spherical tunneling model, there are primarily three components to the total interactive potential between the cluster and the core nucleus: the nuclear, Coulomb, and centrifugal terms [69]

$$V(r) = V_N(r) + V_C(r) + \frac{\hbar^2}{2\mu} \frac{\left(L + \frac{1}{2}\right)^2}{r^2}, \qquad (1)$$

where $V_N(r)$ is represented by a "cosh" geometry of depth V_0, radius R, and nonzero diffuseness a,

$$V_N(r) = -V_0 \frac{1 + \cosh(R/a)}{\cosh(r/a) + \cosh(R/a)}. \qquad (2)$$

L is the angular momentum and the centrifugal barrier is written as its Langer modified form. The three classical turning points can be solved by equation $V(r) = Q_\alpha$ and the radius parameter R can be evaluated for each decay by utilizing the Bohr-Sommerfeld quantization condition [72,73]

$$\int_{r_1}^{r_2} dr \sqrt{\frac{2\mu}{\hbar^2}[Q_\alpha - V(r)]} = (G - L + 1)\frac{\pi}{2}, \qquad (3)$$

where the G is the global quantum number. Under the semiclassical approximation and choosing the appropriate value of the α-cluster preformation factor P_α, we can calculate the α-decay width Γ_s,

$$\Gamma_s = P_\alpha F \frac{\hbar^2}{4\mu} \exp\left[-2 \int_{r_2}^{r_3} dr k(r)\right], \qquad (4)$$

where the F is the normalization factor and $k(r) = \sqrt{\frac{2\mu}{\hbar^2}|Q_\alpha - V(r)|}$. Finally, the α-decay half-life related to the width can be given by $T_{1/2} = \hbar \ln 2/\Gamma_s$.

It is well known that many α emitters are to a certain extent deformed, so it is necessary to consider a deformed tunneling model. For the deformed tunneling model, we choose the deformed density-dependent cluster model [19] to calculate the α-decay width. The α-core potential is expressed as

$$V_{\text{Total}}(R, \beta) = V_N(R, \beta) + V_C(R, \beta) + \frac{\hbar^2}{2\mu} \frac{\left(L + \frac{1}{2}\right)^2}{R^2}, \quad (5)$$

where R is the distance between the centers of mass of the core and the α particle. The orientation angle β is about the α particle with respect to the daughter nucleus symmetry

axis. Using the multipole expansion method, the microscopic potential between the deformable nucleus and the spherical α particle is numerically calculated from the double-folded model

$$V_{N \text{ or } C}(R, \beta) = \sum_{l=0,2,4\dots} V^l_{N \text{ or } C}(R, \beta), \qquad (6)$$

where the multipole component is given by

$$V^l_{N \text{ or } C}(R, \beta) = \frac{2}{\pi}\sqrt{\frac{2l+1}{4\pi}} \int_0^\infty dk k^2 j_l(kR)$$
$$\times \tilde{\rho}_1(k)\tilde{\rho}_2^{(l)}(k)\tilde{v}(k)P_l(\cos\beta). \qquad (7)$$

In multipole components, $\tilde{\rho}_1(k)$ is the Fourier transformation of the α-particle density distribution and $\tilde{\rho}_2^{(l)}(k)$ is the intrinsic form factor. $\tilde{v}(k)$ is the Fourier transformation of the effective interaction about local two-body [74]. After identifying three turning points $R_1(\beta)$, $R_2(\beta)$, $R_3(\beta)$, the decay penetration probability as a function of polar angle can be represented by

$$P_\beta = \exp\left[-2\int_{R_2(\beta)}^{R_3(\beta)} \sqrt{\frac{2\mu}{\hbar^2}|Q_\alpha - V_{\text{Total}}(R, \beta)|}dR\right]. \qquad (8)$$

The α-decay width Γ_d of deformed tunneling model can be obtained by averaging over all directions of P_β,

$$\Gamma_d = P_\alpha F \frac{\hbar^2}{4\mu} \frac{1}{2} \int_0^\pi P_\beta \sin(\theta)d\theta. \qquad (9)$$

Then the half-lives of the deformed tunneling model can be given by $T_{1/2} = \hbar \ln 2/\Gamma_d$.

In the calculation, it is indispensable to determine the P_α, which is a complex process in microscopic computation. Therefore, we use a semiempirical formula to fit the experimental value of the preformation factor P_α^{exp} in five nuclear regions of magicity [36]. The P_α^{exp} is extracted from ratios of experimental decay width to calculated Γ_d, with an assumption that $P_\alpha = 1$ in Eq. (9). The semiempirical formula of the preformation factor used in this paper has the following form [38]:

$$\log_{10}P_\alpha = C_1 N_q + C_2 I_m + C_3\sqrt{l(l+1)} + C_4, \qquad (10)$$

where $N_q = (Z - Z_m)/2$, and $I_m = (N - N_m)/2 - N_q$. Z_m (N_m) represents the nearest magic numbers below Z (N), respectively. l represents the changes of angular momentum between the mother and daughter nuclei and C_{1-4} are the fitting coefficients. Equation (10) contains the quartet number and the magic asymmetry number [38], with an additional angular momentum term to describe unfavored transitions.

B. Bayesian neural network

Bayesian neural network is a probabilistic network, the details of which can be found in Ref. [75]. In this chapter, we only focus on the main features of Bayesian neural network. As the basis for the entire network, Bayes theorem can give the posterior distribution $p(\omega|x, t)$,

$$p(\omega|x, t) = \frac{p(x, t|\omega)p(\omega)}{p(x, t)}, \qquad (11)$$

where $p(\omega)$ is the prior distribution of the ω, $p(x, t|\omega)$ is the likelihood function, and $p(x, t)$ is the marginal likelihood. In our particular case, the x denotes the four input variables, i.e., the proton number Z, the decay energy Q_α, the asymmetric coefficient S, and the change in angular momentum l. The $t = \delta_n$ is the residual of α-decay half-life as

$$\delta_n(\log_{10}T_{1/2}) = \log_{10}\frac{T_{1/2}^{\text{exp}}}{T_{1/2}^{\text{th}}}. \qquad (12)$$

Following the standard practice, assuming a Gaussian distribution to the likelihood function, i.e., $p(x, t|\omega) = \exp(-\chi^2/2)$, where the function $\chi^2(\omega)$ is given by

$$\chi^2(\omega) = \sum_{n=1}^{N}\left[\frac{t_n - S(x, \omega)}{\Delta t_n}\right]^2. \qquad (13)$$

Here, N is the number of available data and Δt_n is the variance parameter of the nth observable. The $S(x, \omega)$ is a function of the neural network which connects input and output through one hidden layer, it can be written as

$$S(x, \omega) = a + \sum_{j=1}^{H} b_j \text{Relu}\left(c_j + \sum_{i=1}^{I} d_{ji}x_i\right), \qquad (14)$$

where $\omega = \{a, b_j, c_j, d_{ji}\}$ are the model free parameters. H is the number of the hidden nodes and I is the number of input variables. The BNN contains four input variables, including the proton number Z, the α-decay energy Q_α, the asymmetric coefficient $S = (N - Z)^2/A$, and the change of angular momentum l. Finally, the function $S(x, \omega)$ consists of a total of $1 + (I + 2)H$ parameters.

The prior distributions $p(\omega)$ is assigned as a zero mean Gaussian function and modeled by a γ distribution. With the prior distribution and likelihood function specified, we make predictions based on the posterior probability density of the neural network averaged over the network parameter ω,

$$\langle S \rangle = \int S(x, \omega)p(\omega \mid x, t)d\omega. \qquad (15)$$

In this paper, we utilize the BNN method to train the residuals directly and construct the internal hidden relationship between the residuals δ_n and characteristic parameters Z, Q_α, S, l. The root-mean-square (rms) deviation σ_{rms} is used to quantify the predictive ability of different models after BNN modification:

$$\sigma_{\text{rms}} = \sqrt{\frac{1}{n}\sum_{i=1}^{n}\left[\log_{10}\left(\frac{T_{1/2}^{\text{exp}}}{T_{1/2}^{\text{th}}}\right)\right]_i^2}. \qquad (16)$$

The architecture of this work and the graphical structure of the BNN is illustrated in Fig. 1. The cubes on the left represent the 479 entire data used for training, which are divided into the learning set and validation set during the extrapolation. The associated interpolation and extrapolation processes are represented by orange and blue arrows, respectively. The panel on the top right shows the structure of the Bayesian neural network used in this work and the formulation description of the Bayes theorem.
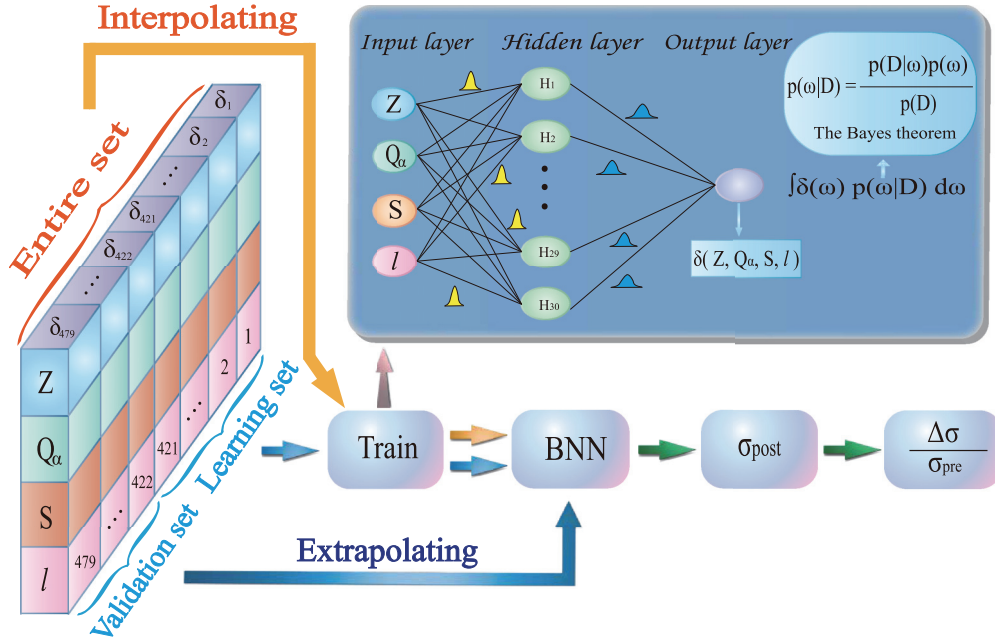
FIG. 1. Pictorial representation of this work. The cubes on the left are the entire set of δ_n regarded as a function of the four characteristic quantities of Z, Q_α, S, l. The orange arrows represent the interpolation process, while the blue arrows represent the extrapolation process.

III. RESULTS AND DISCUSSION

In this part, we analyze the global optimization properties and the extrapolation capabilities of the BNN method to improve the description of model-based predictions of α decay. To pictorially illustrate the fine-tuning of the BNN method in regions affected by shell structure effect, we further present the results for isotopic and isotonic chains. The accuracy of BNN predictions can be guaranteed by utilizing plentiful and accurate experimental data of favored transitions. By introducing the angular momentum term l in BNN inputs, unfavored transitions can be analyzed to explore the hidden nuclear structure information.

A. Global optimization of the BNN method

According to the updated experimental data of Nudat3.0, the entire set containing 479 favored and unfavored α transitions data are incorporated into the training. The raw residuals $\delta_{\text{raw}}(Z, Q_\alpha, S, l)$ for both spherical and deformed tunneling models can be calculated. Then the rms deviations σ_{pre} for the entire set are obtained and listed in Table I. In the calculations,

TABLE I. The rms deviation σ_{pre} of $T_{1/2}$ from the raw spherical tunneling model, the deformed tunneling model and a semiempirical formula, and σ_{post} after BNN corrections. 479 data for favored and unfavored α transitions are chosen as the entire set.

Models	σ_{pre}	σ_{post}	$\Delta\sigma/\sigma_{\text{pre}}$
Sph. mod.	0.882	0.536	39.2%
Defo. mod.	0.776	0.517	33.4%
Sem. form.	0.855	0.545	36.3%

the P_α are acquired through Eq. (10). The coefficients in Eq. (10) are obtained by fitting P_α^{exp} for 479 nuclei across five nuclear regions and are listed in Table II. The P_α^{exp} is given by the ratios of experimental decay width to calculated Γ_d with an assumption that $P_\alpha = 1$. In addition, the result for a semiempirical formula is also presented as a reference in Table I.

Based on the raw residuals $\delta_{\text{raw}}(Z, Q_\alpha, S, l)$, the BNN method is employed to refine the theoretical results to obtain the corrected $T_{1/2}$. The corresponding σ_{post} of the entire set are listed in Table II. In order to measure the improvement of the data set, the relative difference in rms deviation $\Delta\sigma/\sigma_{\text{pre}} = (\sigma_{\text{pre}} - \sigma_{\text{post}})/\sigma_{\text{pre}}$ are also presented in Table I.

From Table I, it can be found that although different decay models have strong robustness and can reproduce the experimental data well, there are still certain deviations between the theoretical $T_{1/2}$ and the experimental data. After BNN corrections, one can see that the BNN method leads to over 30% improvements on the description of model-based predictions of α decay. For the spherical and the deformed tunneling models, the improvements are increased by 39.2% and 33.4%, respectively. These indicate that the BNN method can explore the hidden local half-life correlations between different nuclei and further fine-tune the physical results of the computation. For the semiempirical formula, the prediction accuracy is also improved by 36.3%, which implies that the BNN can improve the predictive ability of the semiempirical formulas by establishing mapping relationships that are difficult to display with explicit expressions. By comparing the data in Table I, it can be concluded that the BNN method is suitable for different types of α-decay models and the prediction accuracy is improved by selecting reasonable feature inputs to physically motivate the network.

TABLE II. Fitted coefficients C_{1-4} of Eq. (10) for preformation factor P_α, which are fitted from 479 data in five different nuclear regions. The number of nuclei in each region is also given.

Regions	$50 < Z < 82$ $50 < N < 82$	$50 < Z < 82$ $82 \leqslant N < 126$	$82 \leqslant Z \leqslant 100$ $82 \leqslant N < 126$	$82 \leqslant Z \leqslant 100$ $N \geqslant 126$	$Z > 100$ $N \geqslant 126$
Numbers	13	101	129	220	16
C_1	0.1616	−0.0251	0.1153	−0.0244	−0.0607
C_2	−0.1859	0.0067	−0.0530	−0.0356	0.0441
C_3	−0.4486	−0.0575	−0.1082	−0.2624	−0.5576
C_4	−0.3394	−0.1413	0.0880	−0.4901	−1.3601

To visually demonstrate the effectiveness of the BNN method for different nuclear regions, the residuals $\delta(Z, Q_\alpha, S, l)$ with and without the BNN corrections are presented in Fig. 2. As can be seen from Figs. 2(a) and 2(b), the regions with large residuals predicted by the spherical and deformed tunneling models always appear in blocks, especially in the superheavy region. After the introduction of the BNN method, the prediction accuracy is improved satisfactorily in the global region.

The theoretical framework of α-decay models mainly include two elements: the α-decay penetration probability and the α-cluster preformation factor P_α. Since we use the experimental Q_α, the calculation of α-decay penetration probability is relatively accurate. As for the P_α, its purely microscopic computation is complicated. In this part, we use Eq. (10) and the coefficients in the Table II to calculate the P_α. Seen from the results of Figs. 2(c) and 2(d), using the BNN method to alter the values of the P_α can improve the description of model-based predictions of α decay.

Combining the results of Table I and Fig. 2, it can be concluded that the BNN method provides reasonable corrections to the P_α by extracting the hidden local effects and makes better prediction accuracy in the global region. The reasons are as follows: first, the four characteristic parameters Z, Q_α, S, l cover the major variation case of α decay, which helps BNN to effectively grasp the changes of P_α from a global perspective. Second, by choosing reasonable numbers of neurons and the
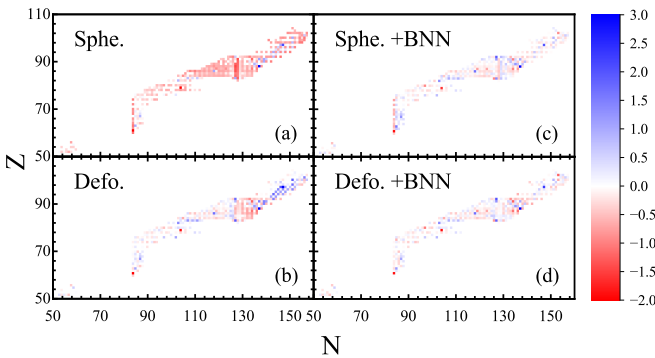
categories of activation functions, the BNN can capture the hidden local correlations between nuclei and obtain important internal physical information, such as shell and pairing effects.

B. Extrapolating capabilities of the BNN method

Extrapolation is more challenging but more appealing than interpolation, especially in the nuclei region where experimental data are very scarce. In this part, we further analyze the extrapolation capabilities of the BNN method in predicting α-decay half-lives. Before the extrapolation, all 479 data in the entire set are divided into the learning set with 421 data and the validation set with 58 data whose $T_{1/2}$ are updated since 2019 in the Evaluated Nuclear Structure Data File (ENSDF) nuclear database [76]. The 58 selected nuclei are uniformly located at the edge of the nuclide diagram in Fig. 2.

First of all, we use the learning set data to determine the value of parameters of the neural network. Once the neural network is calibrated, we calculate the rms deviation and the degree of improvement $\Delta\sigma/\sigma_{\text{pre}}$ of the learning and validation sets. The detailed data are presented in Table III.

For the spherical tunneling model, one can see that it has robust capabilities of global description and extrapolation. With the BNN refinements, the rms deviations of learning set and validation set are improved by 37.7% and 33.0%, respectively. Regarding another deformed tunneling model, the extrapolation ability of the BNN method is also well demonstrated and the rms deviations of learning set and validation set are improved by 33.4% and 21.7%, respectively. It can be considered that the BNN method has reliable extrapolation ability in predicting the α-decay half-lives based on the sophisticated α-decay model.

The results of Table III indicate that the BNN method has effective and reliable extrapolation capabilities. The

FIG. 2. Residuals between logarithm values of theoretical and experimental selected α-decay half-lives. (a) The result of the original spherical tunneling model. (c) The result of spherical tunneling model after BNN correction. (b) The same as in (a) but for deformed tunneling model. (d) The same as in (c) but for deformed tunneling model.

TABLE III. The rms deviation σ_{pre} of $T_{1/2}$ from the theoretical model, and the rms deviation σ_{post} after the BNN corrections. The learning set includes 421 data, and the validation set includes 58 data whose $T_{1/2}$ are updated since 2019 in ENSDF.

Models	Learning set			Validation set		
	σ_{pre}	σ_{post}	$\Delta\sigma/\sigma_{\text{pre}}$	σ_{pre}	σ_{post}	$\Delta\sigma/\sigma_{\text{pre}}$
Sph. mod.	0.868	0.540	37.7%	0.977	0.654	33.0%
Defo. mod.	0.775	0.516	33.4%	0.786	0.615	21.7%
Sem. form.	0.883	0.557	37.0%	0.594	0.480	19.2%
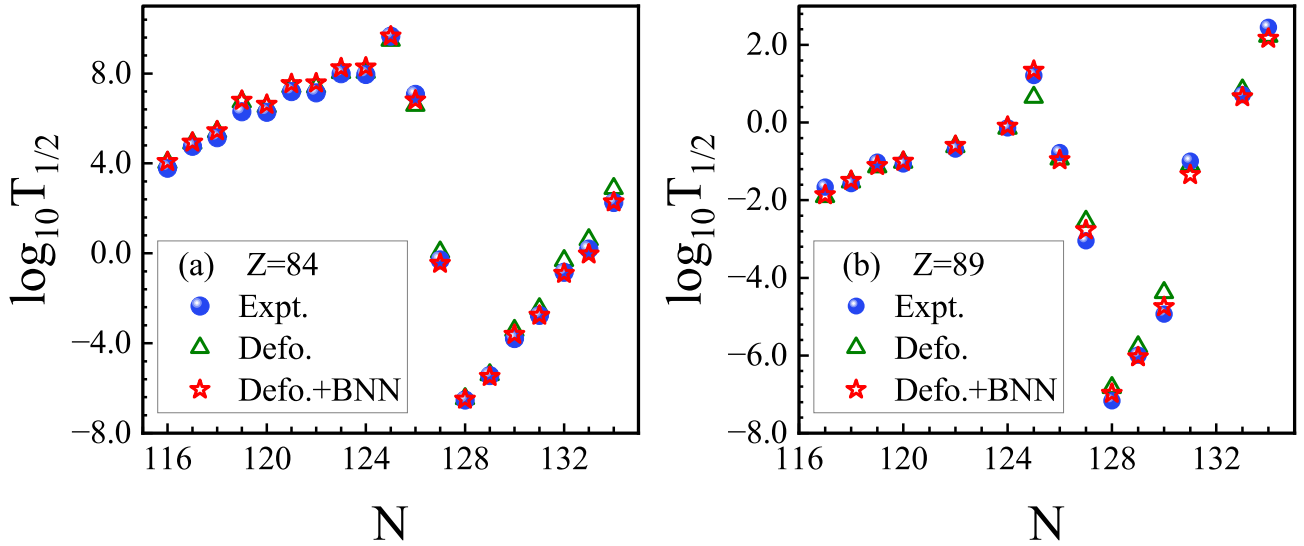
FIG. 3. (a) The logarithm of $T_{1/2}$ for the Po ($Z = 84$) isotopes. The green triangles denote the raw result from the deformed tunneling model, and the red pentacles represent the corrected results from the BNN method. (b) The same as in (a), but for Ac ($Z = 89$) isotopes.

reasons mainly include two aspects. On the one hand, the sophisticated α-decay models are built on the basis of the quantum-tunneling effect. Since the primary physical essence is clearly captured, the decay models can describe the general trend of the changes in α-decay half-lives. On the other hand, the BNN method can detect inner physical interactions in nuclei that cannot be elucidated by parameters in theoretical models. The grasp of details allows BNN to fine-tune the results of the theoretical α-decay models. From the results in Tables I and III, both global and extrapolated results show satisfactory improvements in the description of the α-decay half-lives. Thus, we can use the BNN method to make reliable predictions for the regions lacking experimental data.

C. The BNN refinements for the isotopic and isotonic chains

After illustrating the global descriptions and extrapolating abilities of the BNN method, we further present the refinement behavior of the BNN on $T_{1/2}$ of isotopic and isotonic chains. Although the theoretical models qualitatively reflect the major physical characteristics, there are still some deficiencies in calculating the $T_{1/2}$ affected by the shell structure effect. It is necessary to apply the BNN method to refine the theoretical α-decay models by considering these physical effects more comprehensively.

In the previous discussion, we have demonstrated that the improvements of model description by the BNN method mainly come from the corrections of P_{α}. To pictorially illustrate the performance of the BNN method in refining the P_{α}, we present the $T_{1/2}$ of the deformed tunneling model with and without BNN corrections for $Z = 84$ and 89 isotopic chains in Fig. 3, and for $N = 127$ and 128 isotonic chains in Fig. 4. These figures display the α-decay half-lives of each nucleus with the largest branching ratio. It can be seen from these figures that the theoretical model can give a whole description

of the $T_{1/2}$. When corrected by the BNN method, the refined $T_{1/2}$ achieve more consistent with the experimental data.

In Fig. 3(a), we present the $T_{1/2}$ of even-even and even-odd Po ($Z = 84$) isotopes. It can be seen that, for ^{212}Po ($N = 128$), the deformed tunneling model can reproduce the experimental data well; but for ^{210}Po ($N = 126$) and ^{211}Po ($N = 127$), the descriptions are unsatisfactory due to the inadequate consideration of the shell structure effect. After corrected by the BNN method, the refined $T_{1/2}$ have achieved significant improvements in the descriptions of ^{210}Po and ^{211}Po while retaining the prediction accuracy of ^{212}Po. The discussion of global optimization of the BNN method in Sec. III A has indicated that these corrections mainly come from the refinement of P_{α}. For the ^{211}Po, its preformation factor is adjusted to $P_{\alpha} = 0.026$ after BNN refinement, which is much closer to the result given in Ref. [35].

We further present the $T_{1/2}$ of odd-even and odd-odd Ac ($Z = 89$) isotopes in Fig. 3(b). Compared with the results in Fig. 3(a), there is an overall decrease in describing the $T_{1/2}$ of the Ac isotopic chain calculated by the deformed tunneling model around the shell closures. It can be observed that the deviations between the theoretical $T_{1/2}$ and the experimental data for the nuclei ^{216}Ac ($N = 127$) and ^{217}Ac ($N = 128$) are noticeable due to the influence of the shell structure effect. After the BNN refinements, the theoretical model has greatly improved the descriptions of $T_{1/2}$ of these two nuclei. By the BNN corrections, the preformation factor of ^{216}Ac is adjusted to $P_{\alpha} = 0.034$, which is in good agreement with the result given in Ref. [35]. This indicates that the BNN method combined with the sophisticated α-decay model can well reproduce the $T_{1/2}$ by modifying the value of P_{α} to become more accurately.

Additionally, we present the $T_{1/2}$ of $N = 127$ and 128 isotonic chains in Fig. 4. For the $N = 127$ isotonic chain in Fig. 4(a), the mostly theoretical $T_{1/2}$ is slightly greater than
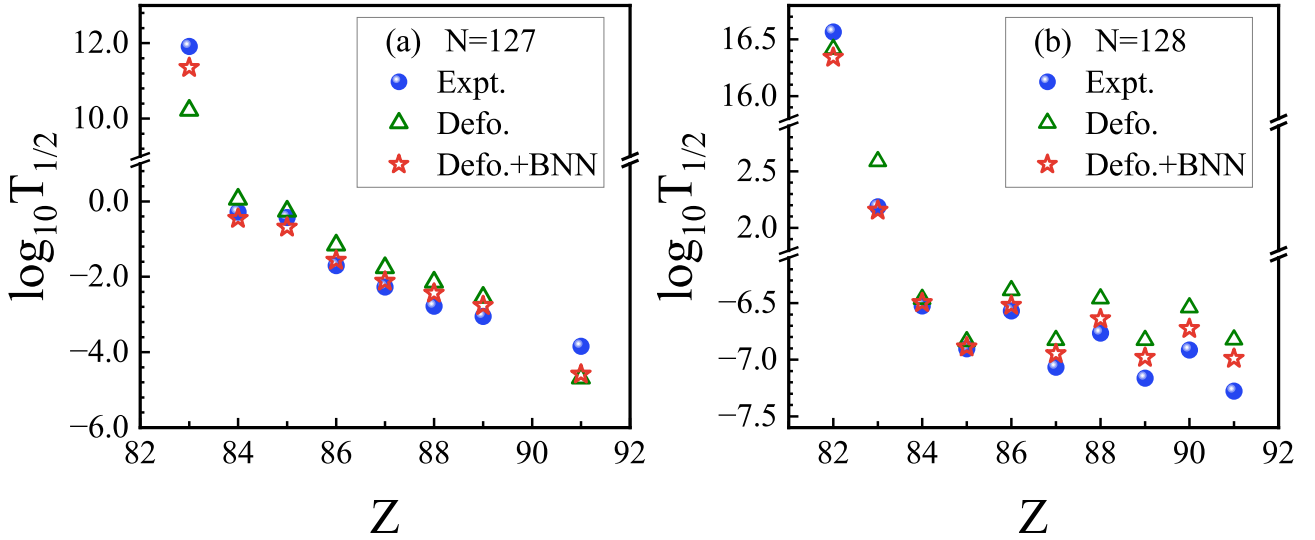
FIG. 4. (a) The logarithm of $T_{1/2}$ for the $N = 127$ isotonic chain. The green triangles denote the raw result from the deformed tunneling model, and the red pentacles represent the corrected results from the BNN method. (b) The same as in (a), but for $N = 128$ isotonic chain.

the experimental data. This is mainly due to the P_α used in raw decay model being generally small in this region. In particular, the $T_{1/2}$ of nuclei ^{210}Bi ($Z = 83$) and ^{211}Po ($Z = 84$) in the shell region are not well presented in the raw decay model. After the BNN refinements, the refined $T_{1/2}$ of $N = 127$ isotonic chains are more consistent with the experimental data overall, especially with a marked improvement around the proton shell $Z = 82$.

For the raw decay model of the $N = 128$ isotonic chain in Fig. 4(b), there are better prediction results for even-even nuclei compared to the even-odd nuclei. This indicates that the P_α in α-decay calculations cannot well reflect the hidden effects of unpaired nucleons. Similar to Fig. 4(a), the $T_{1/2}$ of nuclei ^{210}Pb ($Z = 82$) and ^{211}Bi ($Z = 83$) are not accurately reflected in the theoretical model because of the strong shell effect. When refined by the BNN method, the value of the P_α is modified by further considering the shell and pairing effects. The result demonstrates that the BNN method can acquire the pairing effect and perfectly reproduce the odd-even staggering phenomenon of $T_{1/2}$ in isotonic chains. Combining with the results of Figs. 3 and 4, the BNN method provides rational and convincing corrections to the α-decay half-lives for isotopic and isotonic chains.

IV. SUMMARY

In this work, through the analysis of 479 favored and unfavored α transitions data, we have successfully achieved better half-lives predictions by combining the Bayesian neural network and α-decay models. The intrinsic relationship between Z, Q_α, S, l, and residuals δ are established through the network training. The choice of the experimental Q_α confirms that the improvement of α-decay half-lives with the BNN method comes from the modification of the P_α by capturing essential physical effects. These refinements are clearly

demonstrated in the global and extrapolated analyses of the three selected theories.

For the global optimization of the BNN method, the accuracy of the refined theoretical models has achieved satisfactory improvements, which indicates that the BNN method can provide trustworthy modifications by correcting the value of the P_α. For the extrapolation capabilities, the comparison between the learning set and the validation set shows that the BNN method has robust extrapolating capabilities and can make convincing predictions for the regions lacking experimental data. In addition, through pictorially illustrating the performance of the BNN method in isotopic and isotonic chains, it is more clearly confirmed that the corrections of the P_α come from the accurate grasp of important physical effects such as shell and pairing effects. Generally, our study indicates that the BNN method paves an effective way for describing nuclear decay processes, and has a satisfactory advantage in the evaluation of P_α. It is expected that this work can be applied to other fields of nuclear physics.

[1] D. Vretenar, A. V. Afanasjev, G. A. Lalazissis, and P. Ring, Phys. Rep. **409**, 101 (2005).

[2] T. Otsuka, T. Abe, T. Yoshida, Y. Tsunoda, N. Shimizu, N. Itagaki, Y. Utsuno, J. Vary, P. Maris, and H. Ueno, Nat. Commun. **13**, 2234 (2022).

[3] M. Block, D. Ackermann, K. Blaum, C. Droese, M. Dworschak, S. Eliseev, T. Fleckenstein, E. Haettner, F. Herfurth, F. P. Heßberger *et al.*, Nature **463**, 785 (2010).

[4] J. M. Gates, G. K. Pang, J. L. Pore, K. E. Gregorich, J. T. Kwarsick, G. Savard, N. E. Esker, M. Kireeff Covo, M. J. Mogannam, J. C. Batchelder, D. L. Bleuel, R. M. Clark, H. L. Crawford, P. Fallon, K. K. Hubbard, A. M. Hurst, I. T. Kolaja, A. O. Macchiavelli, C. Morse, R. Orford *et al.*, Phys. Rev. Lett. **121**, 222501 (2018).

[5] N. Kinoshita, M. Paul, Y. Kashiv, P. Collon, C. M. Deibel, B. DiGiovine, J. P. Greene, D. J. Henderson, C. L. Jiang, S. T. Marley *et al.*, Science **335**, 1614 (2012).

[6] S. Peltonen, D. S. Delion, and J. Suhonen, Phys. Rev. C **78**, 034608 (2008).

[7] W. B. He, Y. G. Ma, X. G. Cao, X. Z. Cai, and G. Q. Zhang, Phys. Rev. Lett. **113**, 032506 (2014).

[8] P. E. Hodgson and E. Běták, Phys. Rep. **374**, 1 (2003).

[9] D. E. Ward, B. G. Carlsson, and S. Åberg, Phys. Rev. C **88**, 064316 (2013).

[10] E. M. Ramirez, D. Ackermann, K. Blaum, M. Block, C. Droese, C. E. Düllmann, M. Dworschak, M. Eibach, S. Eliseev, E. Haettner *et al.*, Science **337**, 1207 (2012).

[11] J. Khuyagbaatar, A. Yakushev, C. E. Düllmann, D. Ackermann, L.-L. Andersson, M. Block, H. Brand, D. M. Cox, J. Even, U. Forsberg, P. Golubev, W. Hartmann, R. D. Herzberg, F. P. Heßberger, J. Hoffmann, A. Hübner, E. Jäger, J. Jeppsson, B. Kindler, J. V. Kratz *et al.*, Phys. Rev. Lett. **115**, 242502 (2015).

[12] W. von Oertzen, M. Freer, and Y. Kanada-En'yo, Phys. Rep. **432**, 43 (2006).

[13] L. Wang, J. Liu, R. Wang, M. Lyu, C. Xu, and Z. Ren, Phys. Rev. C **103**, 054307 (2021).

[14] E. Khan, L. Heitz, F. Mercier, and J.-P. Ebran, Phys. Rev. C **106**, 064330 (2022).

[15] G. Gamow, Z. Physik **51**, 204 (1928).

[16] R. W. Gurney and E. U. Condon, Nature **122**, 439 (1928).

[17] Y. Qian and Z. Ren, Phys. Rev. C **90**, 064308 (2014).

[18] M. Ismail and A. Adel, Phys. Rev. C **101**, 024607 (2020).

[19] C. Xu and Z. Ren, Phys. Rev. C **74**, 014304 (2006).

[20] Z. Wang, D. Bai, and Z. Ren, Phys. Rev. C **105**, 024327 (2022).

[21] D. Ni and Z. Ren, Phys. Rev. C **87**, 027602 (2013).

[22] D. S. Delion, Phys. Rev. C **80**, 024310 (2009).

[23] C. Xu, Z. Ren, G. Röpke, P. Schuck, Y. Funaki, H. Horiuchi, A. Tohsaki, T. Yamada, and B. Zhou, Phys. Rev. C **93**, 011306(R) (2016).

[24] S. Yang, C. Xu, G. Röpke, P. Schuck, Z. Ren, Y. Funaki, H. Horiuchi, A. Tohsaki, T. Yamada, and B. Zhou, Phys. Rev. C **101**, 024316 (2020).

[25] S. Yang, C. Xu, and G. Röpke, Phys. Rev. C **104**, 034302 (2021).

[26] P. Mohr, Phys. Rev. C **73**, 031301(R) (2006).

[27] J. Dong, W. Zuo, and W. Scheid, Phys. Rev. Lett. **107**, 012501 (2011).

[28] M. Ismail and A. Adel, Phys. Rev. C **89**, 034617 (2014).

[29] D. S. Delion, R. J. Liotta, and R. Wyss, Phys. Rev. C **92**, 051301(R) (2015).

[30] Y. Qian and Z. Ren, Phys. Lett. B **777**, 298 (2018).

[31] M. Ismail, A. Y. Ellithi, M. M. Selim, N. Abou-Samra, and O. A. Mohamedien, J. Phys. G: Nucl. Part. Phys. **47**, 055105 (2020).

[32] O. N. Ghodsi and M. M. Amiri, Phys. Rev. C **104**, 044618 (2021).

[33] G. Saxena, P. K. Sharma, and P. Saxena, J. Phys. G: Nucl. Part. Phys. **48**, 055103 (2021).

[34] A. N. Andreyev, M. Huyse, P. Van Duppen, C. Qi, R. J. Liotta, S. Antalic, D. Ackermann, S. Franchoo, F. P. Heßberger, S. Hofmann, I. Kojouharov, B. Kindler, P. Kuusiniemi, S. R. Lesher, B. Lommel, R. Mann, K. Nishio, R. D. Page, B. Streicher, Š. Šáro *et al.*, Phys. Rev. Lett. **110**, 242502 (2013).

[35] D. Deng, Z. Ren, D. Ni, and Y. Qian, J. Phys. G: Nucl. Part. Phys. **42**, 075106 (2015).

[36] A. Dumitrescu and D. S. Delion, At. Data Nucl. Data Tables **145**, 101501 (2022).

[37] J.-G. Deng and H.-F. Zhang, Phys. Lett. B **816**, 136247 (2021).

[38] D. S. Delion and A. Dumitrescu, Phys. Rev. C **102**, 014327 (2020).

[39] D. S. Delion and A. Dumitrescu, Phys. Rev. C **103**, 054325 (2021).

[40] S. M. S. Ahmed, R. Yahaya, S. Radiman, and M. S. Yasir, J. Phys. G: Nucl. Part. Phys. **40**, 065105 (2013).

[41] D. Deng and Z. Ren, Phys. Rev. C **93**, 044326 (2016).

[42] S. C. Pieper and R. B. Wiringa, Annu. Rev. Nucl. Part. Sci. **51**, 53 (2001).

[43] R. Roth, T. Neff, H. Hergert, and H. Feldmeier, Nucl. Phys. A **745**, 3 (2004).

[44] T. Neff, H. Feldmeier, and R. Roth, Nucl. Phys. A **752**, 321 (2005).

[45] E. Epelbaum, H. Krebs, D. Lee, and Ulf-G. Meißner, Phys. Rev. Lett. **106**, 192501 (2011).

[46] J. E. Lynn, I. Tews, J. Carlson, S. Gandolfi, A. Gezerlis, K. E. Schmidt, and A. Schwenk, Phys. Rev. C **96**, 054007 (2017).

[47] C. Xu, G. Röpke, P. Schuck, Z. Ren, Y. Funaki, H. Horiuchi, A. Tohsaki, T. Yamada, and B. Zhou, Phys. Rev. C **95**, 061306(R) (2017).

[48] A. Boehnlein, M. Diefenthaler, N. Sato, M. Schram, V. Ziegler, C. Fanelli, M. Hjorth-Jensen, T. Horn, M. P. Kuchera, D. Lee *et al.*, Rev. Mod. Phys. **94**, 031003 (2022).

[49] H. Iwamoto, J. Nucl. Sci. Technol. **57**, 932 (2020).

[50] Z. Yuan, D. Bai, Z. Ren, and Z. Wang, Chin. Phys. C **46**, 024101 (2022).

[51] Y. Ma, C. Su, J. Liu, Z. Ren, C. Xu, and Y. Gao, Phys. Rev. C **101**, 014304 (2020).

[52] Y. Liu, C. Su, J. Liu, P. Danielewicz, C. Xu, and Z. Ren, Phys. Rev. C **104**, 014315 (2021).

[53] C.-Q. Li, C.-N. Tong, H.-J. Du, and L.-G. Pang, Phys. Rev. C **105**, 064306 (2022).

[54] N.-N. Ma, T.-L. Zhao, W.-X. Wang, and H.-F. Zhang, Phys. Rev. C **107**, 014310 (2023).

[55] R. G. Melko, G. Carleo, J. Carrasquilla, and J. I. Cirac, Nat. Phys. **15**, 887 (2019).

[56] T. Vieijra, C. Casert, J. Nys, W. De Neve, J. Haegeman, J. Ryckebusch, and F. Verstraete, Phys. Rev. Lett. **124**, 097201 (2020).

[57] R. Utama and J. Piekarewicz, Phys. Rev. C **97**, 014306 (2018).

[58] L. Neufcourt, Y. Cao, W. Nazarewicz, E. Olsen, F. Viens *et al.*, Phys. Rev. Lett. **122**, 062502 (2019).

[59] I. Kononenko, Biol. Cybern. **61**, 361 (1989).

[60] J. Lampinen and A. Vehtari, Neural Networks **14**, 257 (2001).

[61] R. Utama, W.-C. Chen, and J. Piekarewicz, J. Phys. G: Nucl. Part. Phys. **43**, 114002 (2016).

[62] X.-X. Dong, R. An, J.-X. Lu, and L.-S. Geng, Phys. Rev. C **105**, 014308 (2022).

[63] R. Utama, J. Piekarewicz, and H. B. Prosper, Phys. Rev. C **93**, 014311 (2016).

[64] L. Neufcourt, Y. Cao, W. Nazarewicz, F. Viens *et al.*, Phys. Rev. C **98**, 034318 (2018).

[65] Z. M. Niu, H. Z. Liang, B. H. Sun, W. H. Long, and Y. F. Niu, Phys. Rev. C **99**, 064307 (2019).

[66] F. Minato, Z. M. Niu, and H. Liang, arXiv:2204.06871 (2022).

[67] U. B. Rodríguez, C. Z. Vargas, M. Gonçalves, S. B. Duarte, and F. Guzmán, J. Phys. G: Nucl. Part. Phys. **46**, 115109 (2019).

[68] U. B. Rodríguez, C. Z. Vargas, M. Gonçalves, S. B. Duarte, and F. Guzmán, Europhys. Lett. **127**, 42001 (2019).

[69] C. Xu and Z. Ren, Phys. Rev. C **68**, 034319 (2003).

[70] Z. Y. Wang, Z. M. Niu, Q. Liu, and J. Y. Guo, J. Phys. G: Nucl. Part. Phys. **42**, 055112 (2015).

[71] https://www.nndc.bnl.gov/nudat3/.

[72] B. Buck, A. C. Merchant, and S. M. Perez, Phys. Rev. Lett. **72**, 1326 (1994).

[73] B. Buck, A. C. Merchant, and S. M. Perez, Phys. Rev. Lett. **76**, 380 (1996).

[74] G. Bertsch, J. Borysowicz, H. McManus, and W. G. Love, Nucl. Phys. A **284**, 399 (1977).

[75] R. M. Neal, *Bayesian Learning for Neural Networks* (Springer, Berlin, 1996), pp. 29–53.

[76] https://www.nndc.bnl.gov/ensdf/.